

Photoacoustic absorption spectrometer for highly transparent dielectrics with parts-per-million sensitivity

Niklas Waasem, Stephan Fieberg, Janosch Hauser, Gregory Gomes, Daniel Haertle et al.

Citation: *Rev. Sci. Instrum.* **84**, 023109 (2013); doi: 10.1063/1.4792724

View online: <http://dx.doi.org/10.1063/1.4792724>

View Table of Contents: <http://rsi.aip.org/resource/1/RSINAK/v84/i2>

Published by the [American Institute of Physics](http://www.aip.org).

Related Articles

Electroacoustic response of 1-3 piezocomposite transducers for high power applications
Appl. Phys. Lett. **101**, 253504 (2012)

Three-dimensional micro electromechanical system piezoelectric ultrasound transducer
Appl. Phys. Lett. **101**, 253101 (2012)

Efficient counter-propagating wave acoustic micro-particle manipulation
Appl. Phys. Lett. **101**, 233501 (2012)

Piezoelectric and electrostrictive effects in ferroelectret ultrasonic transducers
J. Appl. Phys. **112**, 084505 (2012)

Piezoelectric resonator arrays for tunable acoustic waveguides and metamaterials
J. Appl. Phys. **112**, 064902 (2012)

Additional information on Rev. Sci. Instrum.

Journal Homepage: <http://rsi.aip.org>


Journal Information: http://rsi.aip.org/about/about_the_journal

Top downloads: http://rsi.aip.org/features/most_downloaded

Information for Authors: <http://rsi.aip.org/authors>

ADVERTISEMENT

JANIS Does your research require low temperatures? Contact Janis today.
Our engineers will assist you in choosing the best system for your application.



10 mK to 800 K LHe/LN₂ Cryostats
Cryocoolers Magnet Systems
Dilution Refrigerator Systems
Micro-manipulated Probe Stations

sales@janis.com www.janis.com
Click to view our product web page.

Photoacoustic absorption spectrometer for highly transparent dielectrics with parts-per-million sensitivity

Niklas Waasem,^{1,a)} Stephan Fieberg,¹ Janosch Hauser,¹ Gregory Gomes,² Daniel Haertle,³ Frank Kühnemann,¹ and Karsten Buse^{1,4}

¹Fraunhofer Institute for Physical Measurement Techniques IPM, Heidenhofstraße 8, 79110 Freiburg, Germany

²University of Toronto, Department of Physics, 60 St. George St., Toronto, Ontario M5S 1A7, Canada

³Matrix Elektronik AG, Kirchweg 24, 5420 Ehrendingen, Switzerland

⁴Department of Microsystems Engineering, University of Freiburg, Georges-Köhler-Allee 102, 79110 Freiburg, Germany

(Received 21 January 2013; accepted 6 February 2013; published online 26 February 2013)

A sensitive photoacoustic absorption spectrometer for highly transparent solids has been built and tested. As the light source an optical parametrical oscillator pumped by a nanosecond pulse laser with 10 Hz repetition rate is employed, covering the complete wavelength range from 407 to 2600 nm. A second-harmonic-generation unit extends the range of accessible wavelengths down to 212 nm. A lead-zirconate-titanate piezo transducer, directly coupled to the sample, detects the photoacoustically generated sound waves. Absorption spectra of lithium triborate, lithium niobate, and alpha barium borate crystals with absorption coefficients down to 10^{-5} cm^{-1} are presented. © 2013 American Institute of Physics. [<http://dx.doi.org/10.1063/1.4792724>]

I. INTRODUCTION

A. Quality control for optical materials

The quality requirements for optical devices rise constantly, either to enhance the performance of existing systems or to enable new applications. High-quality optical materials, such as dielectric substrates, nonlinear optical crystals, or coatings are the basis for most optical devices. Their capabilities often define the upper limit for the performance of optical systems. One critical property of optical materials is light absorption, because the light power deposited inside the medium due to absorption leads to heating and to changes of material properties, e.g., formation of color centers,¹ and – for high light intensities – to physical damage of the materials, e.g., ablation.

Measuring the absorption spectra of optical materials helps to estimate the maximal light intensity the medium can handle, or to distinguish between high and low quality batches. It also gives the opportunity to identify impurities which lead to light absorption, pertinent knowledge for improving the material fabrication process.

Measuring absorption coefficients in highly transparent optical materials is a challenging task. Standard devices such as a Fourier-transform infrared spectrometer (FTIR) or photo spectrometer fail, since they cannot easily detect light extinctions of less than 1%. For this reason, highly sensitive measurement techniques are indirect, they detect the effect of the absorbed light onto the sample, i.e., mostly heating. Laser calorimetry, which became an ISO standard method to determine small absorption coefficients,^{1,2} relies on temperature change directly measured with a thermal detector attached to the edge of the test samples. To detect small absorption, pump lasers with high output power are required. Such lasers

are available only on discrete wavelengths. Thus, no complete absorption spectrum can be recorded. Additionally, calorimetric measurements are rather slow and special sample geometries are required. Alternatively, heating of the illuminated region can be quantified with higher sensitivity by detecting the build up of a thermal lens. Two methods make use of this effect. For photo-thermal common-path interferometry (PCI)³ the profile of a weak probe laser beam is distorted by a thermal lens caused by a strong pump laser beam focused into the center of the probe-beam focus. High continuous-wave (cw) or quasi-cw pump powers are required for this method, measurement times are short (0.1 to 1 s). Another method is laser-induced deflection (LID),⁴ where a probe beam is deflected due to a thermal lens in the vicinity of a strong pump beam. This method also requires high pump powers, it is comparably slow and less sensitive than PCI. With both methods, LID and PCI, surface absorption can be detected and quantified.

Heating due to light absorption does not only lead to the build up of a thermal lens, but also to thermal expansion of the illuminated volume and, for pulsed illumination, to the consequent generation of acoustic waves. Detecting these photoacoustic waves with microphones or piezo transducers is another way to measure small absorptions, named photoacoustic absorption spectroscopy (PAS).⁵ A key advantage of photoacoustic absorption measurements is that pulsed lasers can be used as pump light sources. For ns-pulse lasers optical parametrical oscillators (OPO) became a turn-key commercial product, capable of generating widely tunable light. In this work, the well known photoacoustic effect is exploited for sensitive detection of low absorption, utilizing a ns-OPO system as a tunable pump-light source.

B. Photoacoustic principle

When a dielectric material is illuminated with a light pulse of a few nanoseconds duration, part of the light energy

^{a)}Electronic mail: niklas.waasem@ipm.fraunhofer.de. URL: <http://www.ipm.fraunhofer.de>.

is deposited inside the sample due to light absorption. This is always the case, as there is no dielectric with zero absorption. If the deposited energy is converted into heat, the illuminated region expands thermally. Consequently, an acoustic pressure wave is emitted which propagates to the edges of the sample. The peak pressure P of the acoustic wave has been derived by Tam⁵ for the simple case of cylindrical beam geometries, laser pulse durations shorter than the propagation time of sound across the beam, $\tau_l < R_f/v$, and Gaussian beam profiles

$$P = \frac{\beta v^2}{\pi c_p R_f^{3/2} \sqrt{r}} E_{\text{pulse}} \alpha. \quad (1)$$

Here, β is the thermal expansion coefficient, v is the speed of sound, c_p is the specific heat capacity at constant pressure, R_f is the laser-beam radius, r is the distance from the center of the illuminated cylinder, E_{pulse} is the energy of the laser pulse, and α is the absorption coefficient.

A piezo transducer is attached to the edge of the sample to measure the acoustic pressure P . The piezo voltage U_{piezo} is linearly proportional to the pressure amplitude. Thus, the voltage of the first peak of the piezo signal after illumination U_{PhAc} is proportional to the peak acoustic pressure derived in Eq. (1),

$$U_{\text{PhAc}} = k_{\text{piezo}} P = K E_{\text{pulse}} \alpha \quad (2)$$

with k_{piezo} being a constant which depends on the piezo transducer, on the material of the sample, its geometric orientation, and the coupling between sample and transducer. The calibration coefficient K includes k_{piezo} , material parameters and pump beam properties. The pulse energy E_{pulse} can be measured with a pyro-electric detector. Thus, by finding the calibration coefficient K , the absorption coefficient α can be determined as

$$\alpha = \frac{U_{\text{PhAc}}}{E_{\text{pulse}} K} = \frac{S_{\text{PhAc}}}{K} \quad (3)$$

with $S_{\text{PhAc}} = U_{\text{PhAc}}/E_{\text{pulse}}$ being the normalized photoacoustic signal.

The calibration coefficient K cannot be calculated theoretically using Eqs. (1) and (2), since the impedance matching of the acoustic waves from the sample material into the piezo transducer is unknown. Consequently, the absorption calibration of the photoacoustic spectrometer, i.e., determining K , requires reference data.

II. SETUP

In this section the optical setup of the photoacoustic spectrometer is described. All important components are listed, scan and read-out algorithms are explained.

A. Light source

To obtain absorption spectra, a tunable light source is required. Here, an OPO from GWU-Lasertechnik (versaScan/500/MB) is employed to generate light in the wavelength range 407–2600 nm. The OPO is pumped by the third harmonic (355 nm) of a 1064-nm nanosecond Nd:YAG

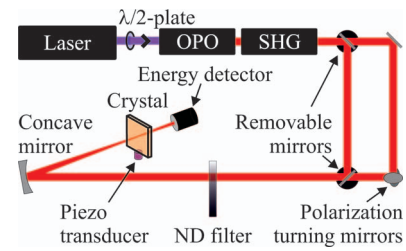


FIG. 1. Experimental setup: Light pulses are generated and focused onto a sample. A piezo transducer is attached to the sample to measure the acoustic signal.

pulse laser. The linewidth of the OPO output is $2\text{--}7\text{ cm}^{-1}$, even at the degeneration point (710 nm). A second-harmonic-generation (SHG) unit also from GWU-Lasertechnik (uvScan) is applied for frequency doubling of the OPO output, expanding the wavelength range down to 212 nm. Typical output pulse energies are in the mJ regime, the pulse duration is $7.5(\pm 1)\text{ ns}$.

The polarization of the OPO beam can be turned by a polarization turning mirror set. The pulse energy is attenuated by variable neutral density filters or by using a half-wave plate which turns the polarization of the pump light for the OPO, see Fig. 1. A concave mirror focuses the laser pulses achromatically into the sample to a beam diameter of 1 mm (FWHM) at the sample position. The pulse energy is monitored by a pyro-electric energy detector (Newport 818E-03-12-L) placed behind the sample.

B. Detection – piezo transducer and read out

A PCB 132A35 piezo transducer detects the photoacoustic pressure waves. Samples are put onto the transducer and fixed with two plastic screws. The minimal dimensions of a sample for direct coupling are $12 \times 2 \times 0.5\text{ mm}^3$. For indirect coupling, i.e., using an acoustic waveguide between sample and piezo transducer,⁵ $3 \times 2 \times 1\text{ mm}^3$ is sufficient. The entrance and exit planes of the sample must be polished. Glycerol is used to enhance acoustic coupling between sample and piezo transducer. Glycerol also helps to enhance the reproducibility of the coupling to $\pm 20\%$. It was measured by remounting one sample onto the piezo transducer several times.

The piezo signal is amplified (Femto voltage amplifier, series HVA) and sent through a passive band-pass filter (cut-off frequencies are 0.2 and 2 MHz). The resulting signal is measured and digitized with an oscilloscope (LeCroy Wave-master 8300A). A typical photoacoustic signal, Fig. 2, occurs with a delay of $\tau_{\text{delay}} = r/v$ owing to the sound velocity v for longitudinal waves inside the sample. The oscillation of the sample and the holder is weakly damped, the amplitude remains nearly constant. The shape of the signal depends on various parameters such as geometry of the sample, place of excitation, piezo transducer, and coupling, but is maintained for all intensities and wavelengths. The amplitude of the piezo signal depends linearly on the pulse energy, as long as the light intensity is sufficiently low to avoid nonlinear absorptions in the sample, Fig. 3. With the shape of the signal staying the same, the amplitude of the photoacoustic voltage U_{PhAc} is proportional to the amplitude of each point of the

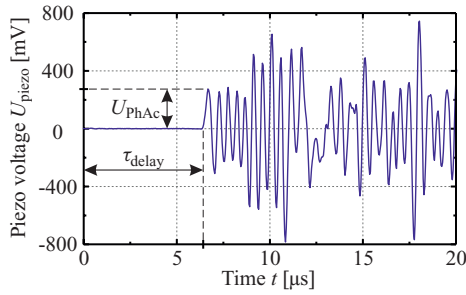


FIG. 2. Typical photoacoustic signal measured with the piezo transducer, the sample is an undoped congruent lithium niobate crystal with dimensions $(x \times y \times z) = 1 \times 60 \times 10 \text{ mm}^3$. The distance between transducer and illuminated cylinder is 40 mm, leading to a delay of $\tau_{\text{delay}} = r/v = 6.5 \mu\text{s}$. The measured quantity is the maximal voltage of the first peak U_{PhAc} , called the photoacoustic voltage.

photoacoustic signal $U_{\text{piezo}}(t)$ after excitation of the acoustic wave. The photoacoustic voltage U_{PhAc} is defined as the maximal piezo voltage of the first peak. The first peak is chosen because Eq. (1) describes it. Nonetheless, the rest of the measured signal is used to enhance the signal-to-noise ratio by applying a matched filter algorithm: first, for a wavelength with a high absorption coefficient α , a clear and noiseless reference signal $R(t)$ is measured and stored in the memory of the oscilloscope. Second, the reference signal $R(t)$ is used to distinguish between photoacoustic signal and noise, by calculating

$$U_{\text{PhAc}}^{\text{correl}} = U_{\text{PhAc}}^R \frac{\int S(t)R(t)dt}{\int R(t)R(t)dt}. \quad (4)$$

Here, $U_{\text{PhAc}}^{\text{correl}}$ is the so-called correlated photoacoustic voltage, U_{PhAc}^R is the maximal amplitude of the first peak of the reference signal $R(t)$, $S(t)$ is the measured signal, and t is the time, starting with the arrival time of the laser pulse ($t = 0$). The integration starts at $t = \tau_{\text{delay}}$ and ends at $t = 50 \mu\text{s}$. Since the oscilloscope digitizes the measured signal, $S(t)$ and $R(t)$ are discrete, the integration in Eq. (4) is technically a scalar product

$$U_{\text{PhAc}}^{\text{correl}} = U_{\text{PhAc}}^R \frac{\sum_i S(t_i)R(t_i)}{\sum_i R(t_i)R(t_i)} = U_{\text{PhAc}}^R \frac{\langle R \times S \rangle}{\langle R \times R \rangle}. \quad (5)$$

All operations are made in real time by the oscilloscope. Both values, $U_{\text{PhAc}}^{\text{correl}}$ and U_{PhAc} , are read out and stored for each wavelength measured.

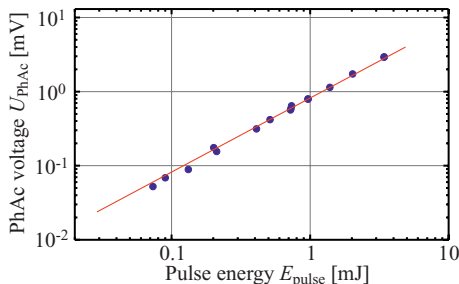


FIG. 3. The photoacoustic voltage rises linearly with pulse energy, shown here for a lithium triborate crystal and y-polarized light at 1600 nm wavelength.

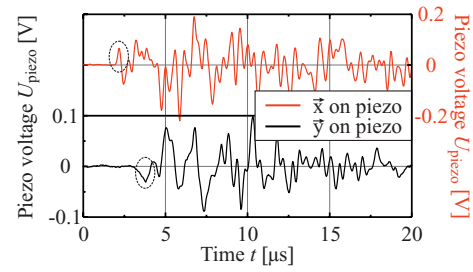


FIG. 4. Photoacoustic signal for an LBO crystal, top: crystallographic \bar{x} axis points onto the piezo, bottom: \tilde{y} axis points onto the piezo.

The setup is fully automated. A LABVIEW-based software sets the desired wavelength of the OPO and the pulse energy using the ND filter, it records the pulse energy with the pyroelectric detector, and reads out the oscilloscope. Typical measurement times are 12 s for each wavelength and 45 min for a complete wavelength scan from 410 to 2600 nm with a step size of 10 nm.

III. PERFORMANCE

Absorption spectra of several optical materials are recorded to assess the performance of the photoacoustic spectrometer. In this section, absorption spectra of two important nonlinear optical materials and one highly transparent linear optical material are presented.

A. Lithium triborate

Lithium triborate (LBO) crystals are employed for second-harmonic generation of infrared laser light into the visible range, because of their wide transmission window from 160 to 2600 nm and their extremely high damage threshold, being larger than 45 GW/cm^2 for ns-pulses at $1 \mu\text{m}$ wavelength.⁶ However, the large thermal expansion coefficients of LBO are a drawback for applications. If the crystal heats up in the illuminated region due to light absorption, the crystal expands along the crystallographic x axis ($\beta_x = 10.8 \times 10^{-5}/\text{K}$) and shrinks along the y axis ($\beta_y = -8.8 \times 10^{-5}/\text{K}$). This causes internal stress changing the material properties which consequently leads to phase mis-matching. The different sign of β for the x and y axes can be observed experimentally. If a y - z -plane of the LBO crystals is put onto the piezo transducer, i.e., the crystallographic \bar{x} axis points onto the piezo, the first peak of the photoacoustic signal has a positive sign and for the \tilde{y} axis orientation the sign is negative, see Fig. 4. For all other geometries and materials shown in this paper, a positive first peak is observed, like in Fig. 2.

1. Calibration

LBO crystals exhibit high absorption in the wavelength range around 2400 nm, which can be measured by independent techniques, photoacoustically and using a FTIR spectrometer. A comparison of the measurements yields a calibration coefficient K . The calibration for ordinary light

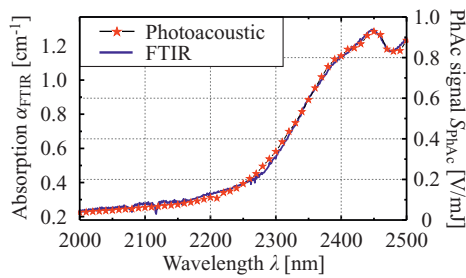


FIG. 5. Calibration: The photoacoustic measurement is compared to the absorption spectrum measured with a FTIR spectrometer. The comparison yields the calibration coefficient, to convert the normalized photoacoustic signal into absorption coefficients.

polarization is illustrated in Fig. 5. The absorption rises for light of longer wavelengths, exhibiting an absorption peak at 2450 nm with $\alpha = 1.3 \text{ cm}^{-1}$. The ordinate scale of the FTIR measurement is aligned to match the photoacoustic and FTIR spectra. The offset of 0.18 cm^{-1} on the FTIR scale can be explained by the absolute inaccuracy of the measurement which is 2%. A systematic deviation of this size is normal for direct absorption-measurement techniques. The increased extinction may be caused by an imperfect cleaning of the surface of the sample, or due to a shift of the light power emitted by the lamp, or a not-perfect Fresnel-reflection correction, due to imprecise knowledge of the refractive indices or due to a slightly tilted alignment of the sample with respect to the probe-beam direction. The photoacoustic spectral fingerprint agrees with that of the FTIR measurement. The obtained calibration coefficient for this measurement is $K_{\text{LBO}} = 840(\pm 30) \text{ cm V/J}$.

2. Absorption spectra

Figure 6 shows the photoacoustic absorption spectrum of an LBO crystal for light polarized along the crystallographic y axis. The absorption coefficient α is around 10^{-5} cm^{-1} within 500–1200 nm wavelength range. For wavelengths between 1200 and 2600 nm the absorption coefficient increases by about five orders of magnitude. This steep rise of α is attributed to multi-phonon absorption.⁷ For wavelengths below 500 nm the absorption coefficient rises also. A comparison of crystals from different suppliers, Fig. 7, discloses substantially different absorption values in the range below 550 nm, while the absorption spectra are identical in the infrared regime for wavelengths above 1500 nm. In this range,

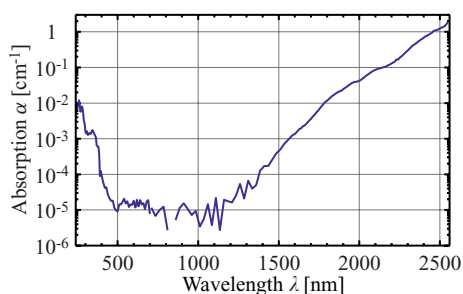


FIG. 6. Photoacoustic absorption spectrum of an LBO crystal (sample 4) for light polarized along the crystallographic y axis.

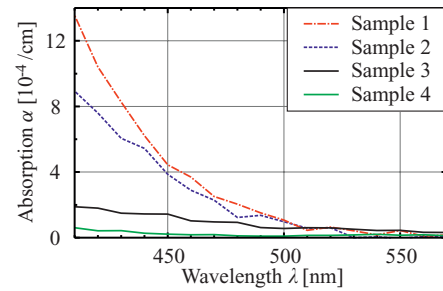


FIG. 7. Comparison of photoacoustic absorption spectra of LBO crystals from different growers for light polarized along the crystallographic y axis.

multi-phonon absorption sets a fundamental limit to the maximal transparency of LBO crystals. Consequently, a further reduction of the absorption coefficients cannot be achieved.

In the wavelength range below 500 nm, samples 1, 2, and 3 exhibit higher absorption levels than sample 4. Thus, a further improvement of the fabrication process would yield lower absorption and possibly better performance of those crystals.

B. Lithium niobate

Crystalline lithium niobate (LiNbO_3) is one of the most important materials for nonlinear optics. It is used, e.g., for cw OPOs⁸ or for SHG of cw laser light at 1 μm wavelength into the green spectral range.⁹ A key advantage are the large nonlinear optical coefficients. Absorption due to residual impurities, such as Fe, Cr, or OH^- can be an obstacle for applications. It has been shown that mid-infrared absorption bands can inhibit OPO operation.¹⁰ After annealing the crystals, those bands vanished and the OPO performed as desired.

LiNbO_3 crystals also show the photorefractive effect which is, along with absorption, another obstacle for high-power applications. The origin of the photorefractive effect in LiNbO_3 is the redistribution of electrons, trapped, e.g., at residual Fe impurities, due to excitation by light absorption. The photorefractive Fe^{2+} centers can be detected in the absorption spectrum. There are two prominent absorption bands, one around 500 nm and the other one between 1000 and 1400 nm.¹¹ The concentration of Fe^{2+} ions can be determined by measuring the absorption coefficient.

1. Calibration

The multi-phonon-absorption band of LiNbO_3 crystals cannot be applied for absorption calibration, since it is shifted to longer wavelengths than in LBO. The only pronounced absorption feature is caused by hydrogen impurities which form OH^- groups. Excitation of the fundamental OH^- vibration leads to a strong absorption band centered at 2871 nm,¹⁰ Fig. 8. This absorption band is not within the accessible wavelength range of the OPO. Thus, it cannot be applied for direct calibration. There are no other absorption features in the transmission window of undoped LiNbO_3 crystals that can be measured with a standard grating or Fourier transform absorption spectrometer. The band-to-band absorption in the UV range cannot be used for calibration because of

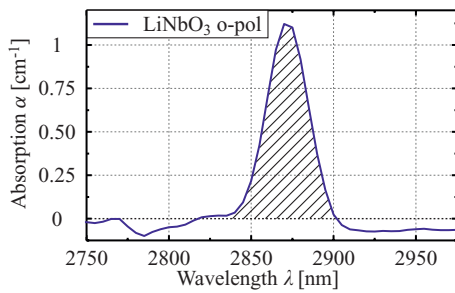


FIG. 8. Calibration: The absorption band of the fundamental OH^- vibration can be measured with a standard grating spectrophotometer.

substantial two-photon absorption, see Sec. IV A. For this reason, direct absorption calibration is not possible for LiNbO_3 crystals. However, the OH^- groups exhibit overtone vibrations that can be excited by light of shorter wavelength. The absorption band of the first overtone is centered at 1475 nm,^{12,13} it can be measured with the photoacoustic setup, see Fig. 9. The background absorption (dotted line) is caused by Fe impurities. It is known from literature that the oscillator strength of the first overtone is a factor of 200 smaller than that of the fundamental process, for MgO-doped LiNbO_3 the factor is 175.^{12,13} Thus, the calibration coefficient K can be derived by comparing the grating-spectrometer measurement of the fundamental absorption band, Fig. 8, with the photoacoustic measurement of the first overtone, Fig. 9. The calibration coefficient obtained for the measurement presented here is $K_{\text{LN}} = 120(\pm 25) \text{ cmV/J}$.

2. Measurement

The band gap of LiNbO_3 crystals is 3.7 eV. Thus, two-photon absorption must be considered for photon-energies larger than 2 eV (wavelengths shorter than 600 nm) at high light intensities. In Fig. 10 the photoacoustic signal at 532 nm wavelength is plotted versus pulse energy. For small pulse energies, the photoacoustic signal rises linearly, like in Fig. 3. For pulse energies larger than 0.8 mJ the photoacoustic signal starts to rise quadratically with intensity, here two-photon absorption dominates linear absorption. This behavior must be considered for the photoacoustic measurement of the absorption spectra. Pulse energies well below 0.3 mJ must be used to reliably measure the linear absorption coefficient for

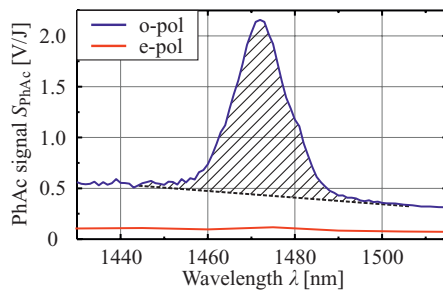


FIG. 9. Calibration: The absorption band of the overtone of the OH^- vibration can be measured with the photoacoustic spectrometer. The ratio of the oscillator strengths between fundamental and overtone vibration is known from literature.

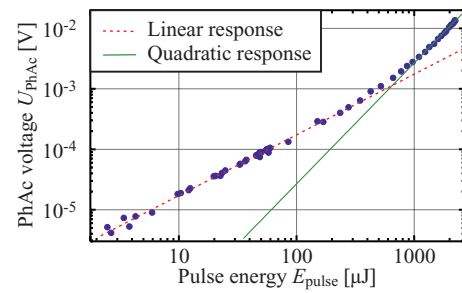


FIG. 10. Photoacoustic signal of a LiNbO_3 crystal versus laser pulse energy at 532 nm wavelength. For high pulse energies two-photon absorption dominates linear absorption.

wavelengths around 532 nm. For photon energies closer to the band-gap energy, i.e., shorter wavelengths, the two-photon-absorption coefficient β_{TPA} becomes even larger.¹⁴

3. Absorption spectra

The absorption spectrum of an undoped congruent LiNbO_3 crystal for ordinary and extraordinary light polarization is shown in Fig. 11. The absorption coefficient starts at a level of 10^{-1} cm^{-1} between 400 and 500 nm. This absorption can be attributed to Fe^{2+} impurities.¹¹ For larger wavelengths the absorption drops to a minimum of 10^{-3} cm^{-1} for ordinary polarization and to $2 \times 10^{-4} \text{ cm}^{-1}$ for extraordinary light polarization around 1700 nm. For wavelengths near the degeneracy point of the OPO at 710 nm, the noise level of the absorption data rises. This is because the OPO output power is low and signal and idler light are difficult to separate in this range. For ordinary polarization a broad absorption band between 900 and 1500 nm and a sharp absorption peak at 1472 nm are observed. The broad absorption band can be attributed to Fe^{2+} impurities, while the sharp absorption peak is the overtone of the OH^- absorption band which is employed for calibration, see Fig. 9. As expected, both bands are visible for ordinary polarization only. For wavelengths above 2100 nm, the absorption level rises and additional sharp absorption bands are detected with peaks centered at 2255, 2310, and 2487 nm wavelength for both polarizations. Those absorption bands have been observed earlier by Schweswy *et al.*,¹⁰ they are attributed to a mixed OH^- stretching and libration transitions.¹⁵

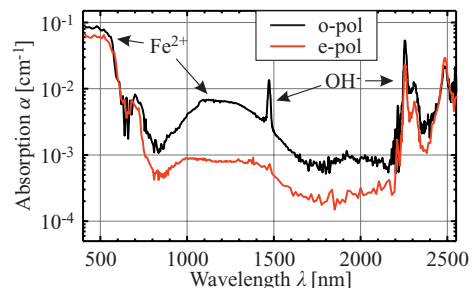


FIG. 11. Absorption spectrum of an undoped LiNbO_3 crystal for ordinary and extraordinary polarization, measured with the photoacoustic absorption spectrometer.

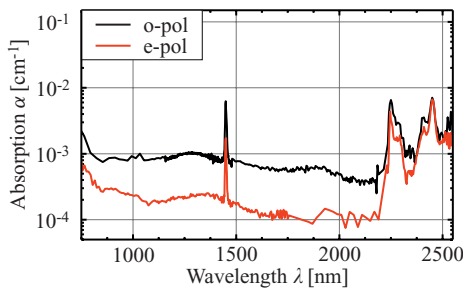


FIG. 12. Absorption spectrum of a 5 mol.% MgO-doped LiNbO₃ crystal for ordinary and extraordinary light polarization, measured with the photoacoustic absorption spectrometer.

4. Magnesium-doped lithium niobate

Doping LiNbO₃ with more than 5 mol.% MgO (MgLN) is a standard technique to suppress both the photorefractive effect¹⁶ and green-induced infrared absorption.¹⁷ It is also known that MgLN crystals exhibit lower absorption than undoped crystals. Figure 12 shows absorption spectra of a MgLN crystal for ordinary and extraordinary light polarization. The absorption spectra of MgLN are similar to those of undoped congruent LiNbO₃ in Fig. 11, differences are: (1) For ordinary polarization, the Fe²⁺ band between 900 and 1500 nm is strongly suppressed, (2) The OH⁻ vibration overtone can also be seen in extraordinary polarization, (3) The absorption bands originating from hydrogen impurities are shifted by roughly 30 nm towards shorter wavelengths. All differences to undoped congruent LiNbO₃ are expected.^{13,16,18} In Fig. 13 the absorption bands at 2250, 2285, 2410, and 2450 nm are illustrated. They are attributed to a combination of stretching and libration of OH⁻ ions.¹⁵ Those absorption bands can be suppressed by annealing the crystal.¹⁰

C. Alpha barium borate

Alpha barium borate (α -BBO) is a highly transparent crystal, typically employed for high-power polarizers because of its large birefringent coefficients and its wide transmission window. In contrast to β -BBO, it is optically linear.

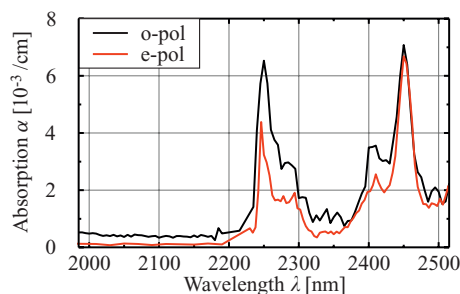


FIG. 13. Absorption bands of a 5 mol.% MgO-doped LiNbO₃ crystal between 2000 and 2500 nm wavelength.

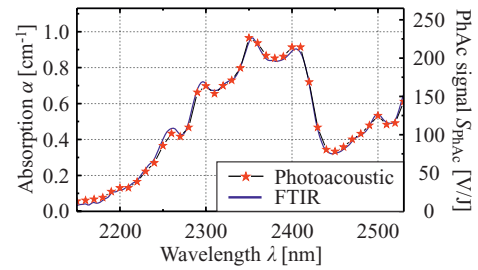


FIG. 14. Absorption spectra of α -BBO measured with the photoacoustic setup and with a FTIR spectrometer.

1. Calibration

For wavelengths above 2200 nm, α -BBO shows absorption bands perfectly suited for calibrating the photoacoustic setup, Fig. 14. The calibration coefficient obtained for the photoacoustic measurement of α -BBO presented here is $K = 235(\pm 8)$ cmV/J.

2. Absorption spectrum

The absorption spectrum of the α -BBO crystal is shown in Fig. 15. In the visible range, the absorption drops from 3×10^{-2} cm⁻¹ at 410 nm to 2×10^{-3} cm⁻¹ at 700 nm. Between 730 and 1600 nm, absorption coefficients are lower than 10^{-3} cm⁻¹, the minimum is 10^{-4} cm⁻¹ between 1100 and 1350 nm. Between 1350 and 2350 nm the absorption-coefficient level increases about four orders of magnitude. In this range, additional distinct absorption bands are found at wavelengths 1800, 1960, and 2090 nm, see Fig. 15.

IV. DISCUSSION

Handling, calibration, and performance of the new photoacoustic spectrometer are discussed in this section, on the basis of the experiences made with the three materials tested.

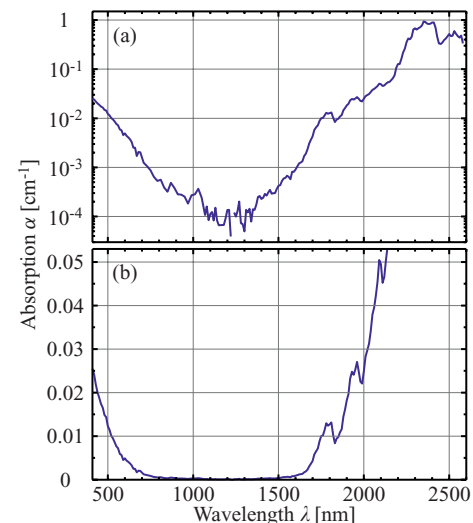


FIG. 15. Absorption spectrum of an α -BBO crystal for ordinary light polarization, (a) in semi-logarithmic scale, (b) in linear ordinate scale. Absorption bands at 1800, 1960, and 2090 nm are measured with the photoacoustic setup.

A. Calibration

One of the most important issues for all highly-sensitive absorption-measurement techniques is the absolute calibration. The photoacoustic spectrometer provides a wide spectral range, 212–2600 nm, which is a substantial advantage for calibration. If absorption bands are present in this range which can be measured both photoacoustically and employing a standard spectrometer, calibration coefficients can be determined in a simple manner: comparison of both spectra yields calibration coefficients with a reproducibility of more than 97% for consecutive measurements. This is the case, e.g., for LBO and α -BBO crystals.

The calibration for LiNbO₃ crystals is more challenging, since there are no absorption bands in the infrared wavelength range below 2600 nm, which can be measured with a standard spectrometer. The UV absorption edge of LiNbO₃ at 350 nm can be measured with a grating photo spectrometer. In this wavelength range, however, it is extremely challenging to measure linear absorption coefficients with the photoacoustic spectrometer, since for photon energies close to the width of the band gap, two-photon-absorption coefficients are very high. Since the intensity range of the ns-laser pulses is high compared to typical cw intensities, two-photon absorption dominates over linear absorption in this range. Thus, the band-absorption edge cannot be used for calibration. Consequently, we chose the overtone absorption band of an OH⁻ vibration for calibration. The absorption value of this band can be calculated by measuring the fundamental absorption band at 2871 nm wavelength, because the relative oscillator strengths of fundamental and overtone excitations are known. The error of this indirect calibration is about 20% of the absolute value.

For the LiNbO₃ measurement we got the smallest calibration coefficient ($K = 120$ cmV/J) and for LBO the largest (840 cmV/J). The reason is mainly because LBO exhibits higher thermal expansion coefficients ($\beta_x^{\text{LBO}} = 101 \times 10^{-6}/\text{K}^{19}$) than LiNbO₃ ($\beta_c^{\text{LiNbO}_3} = 6 \times 10^{-6}/\text{K}^{20}$), while the sound velocities and specific heat capacities are comparable ($v^{\text{LBO}} = 7 \times 10^3$ m/s,²¹ $c_p^{\text{LBO}} = 1$ J/g/K,²² $v_c^{\text{LiNbO}_3} = 7 \times 10^3$ m/s,²⁰ and $c_p^{\text{LiNbO}_3} = 0.6$ J/g/K²³).

B. Detection limit

Its high sensitivity is the main advantage of the photoacoustic spectrometer compared to standard optical spectrometers. Absorption coefficients of the order of 10^{-5} cm⁻¹ have been measured in 1-mm-thick LBO crystals, i.e., 1 ppm of the incident 10-mJ-light-pulse energy converted into heat (10 nJ per pulse) can be detected with averaging over 600 pulses. The detection limit scales inversely with the calibration coefficient of the material and with the maximal pulse energy provided by the OPO for each wavelength. Using these values, the achieved practical detection limit can be estimated as

$$\alpha_{\min}(\lambda) \approx \frac{10^{-4}}{E_{\text{pulse}}(\lambda)K} [\text{cm}^{-1}] \quad (6)$$

with the pulse energy $E_{\text{pulse}}(\lambda)$ given in J and the calibration coefficient K given in cmV/J. The maximal output pulse

energy of the OPO is 0.1 J at 450 nm wavelength. Thus, for materials with $K = 10^3$ cmV/J the sensitivity of the photoacoustic spectrometer is in the 1–10 ppm/cm range at that wavelength.

The sensitivity is lower for wavelengths where the OPO has a lower output power (212–216 nm; 350–406 nm; 690–730 nm; 2000–2600 nm). Best sensitivities are achieved between 410 to 600 nm and 900 to 1600 nm.

A further enhancement of the sensitivity can be reached by increasing the time for averaging. Nonetheless, for LBO crystals the detection limit is determined by the effect of pump light that is scattered in the sample, hitting the piezoelectric transducer and generating an additional signal $S_{\text{sca}}(t)$, consequently. The $S_{\text{sca}}(t)$ can be distinguished from the pure photoacoustic signal $S(t)$, because it starts right after the laser pulse is emitted, i.e., without delay time τ_{delay} that the acoustic wave needs to reach the detector. Also, the scalar product $\langle R \times S_{\text{sca}} \rangle$ is typically three orders of magnitude smaller than $\langle R \times S \rangle$, for the same peak-to-peak values of $S_{\text{sca}}(t)$ and $S(t)$. Thus, $S_{\text{sca}}(t)$ affects $U_{\text{PhAc}}^{\text{correl}}$ only little, but sets the detection limit for low absorption coefficients.

The detection limit of other sensitive methods, such as laser calorimetry,^{1,2} photo-thermal common-path interferometry (CPI),³ and LID,⁴ is also in the 1–10 ppm/cm range, depending on the accessible pump-laser power and material coefficients. In contrast to photoacoustic detection, CPI and LID are more sensitive for materials with high thermo-optic coefficients, e.g., LiNbO₃, potassium titanyl phosphate (KTP), and sapphire (Al₂O₃), while photoacoustic methods are sensitive for materials with high thermal-expansion coefficients, such as LBO, potassium dihydrogen phosphate (KDP), and bismuth borate (BiBO).

C. Limitations

The photoacoustic detection is sensitive only to absorption processes which lead to a thermal relaxation of the states excited by the absorption of a photon, and thus, to heating. The thermal-relaxation time must be at the timescale of the detection, i.e., 10^{-6} s, or faster. Absorption processes leading to electrons in metastable states or to states which exhibit a strong luminescence de-excitation channel show smaller photoacoustic response. In this case, the photoacoustic measurement underestimates the actual absorption coefficient. However, a very good agreement of the qualitative shape has been observed for all absorption features measured with the photoacoustic spectrometer, which have been compared to FTIR or grating spectrometer data.

Another effect which might influence the photoacoustic detection for very small absorption coefficients is electrostriction. The electrostrictive effect would lead to a wavelength-independent contribution to the normalized photoacoustic signal, i.e., an offset. However, we have not found any evidence for an electrostrictive contribution so far. A detailed discussion about electrostriction and its contribution to photoacoustic measurements can be found in literature.^{24,25}

The photoacoustic spectrometer allows measurements of bulk absorption coefficients in solids. A separation of surface and bulk contribution is not possible with the current setup.

Thus, absorption of coatings or surface absorption cannot be measured separately.

V. SUMMARY

A new and very sensitive photoacoustic absorption spectrometer for highly transparent solids is presented. A piezoelectric transducer coupled directly to the sample measures photoacoustic sound waves. An OPO pumped by a ns-pulse laser at 355 nm is employed to generate tunable light in the wavelength range 407–2600 nm, a subsequent SHG unit covers the wavelength range 212–406 nm. Absorption spectra of three different highly transparent optical materials (LBO, LiNbO₃, and α -BBO) are recorded. Calibration coefficients are determined for all materials, enabling the transformation of the normalized photoacoustic signal into absolute absorption coefficients. All absorption bands measured, both with the photoacoustic spectrometer and employing standard techniques, show the same qualitative behavior. In LBO crystals the lowest absorption coefficient measured is 10^{-5} cm^{-1} at $1 \mu\text{m}$ wavelength.

ACKNOWLEDGMENTS

Financial support of the Deutsche Forschungsgemeinschaft is gratefully acknowledged.

¹E. Eva and K. Mann, *Appl. Phys. A* **62**, 143 (1996).

²“ISO 11551:2003 optics and optical instruments – lasers and laser-related equipment – test method for absorptance of optical laser components”.

- ³A. Alexandrovski, M. Fejer, A. Markosyan, and R. Route, in *Solid State Lasers XVIII: Technology and Devices*, Vol. 7193, edited by W. A. Clarkson, N. Hodgson, and R. K. Shori (SPIE, Bellingham, 2009).
- ⁴C. Mühlig, W. Triebel, S. Kufert, and S. Bublitz, *Appl. Opt.* **47**, C135 (2008).
- ⁵A. C. Tam, *Rev. Mod. Phys.* **58**, 381 (1986).
- ⁶Y. Furukawa, S. A. Markgraf, M. Sato, H. Yoshida, T. Sasaki, H. Fujita, T. Yamanaka, and S. Nakai, *Appl. Phys. Lett.* **65**, 1480 (1994).
- ⁷M. Sparks and L. J. Sham, *Phys. Rev. B* **8**, 3037 (1973).
- ⁸I. Breunig, D. Haertle, and K. Buse, *Appl. Phys. B* **105**, 99 (2011).
- ⁹P. A. Franken, G. Weinreich, C. W. Peters, and A. Hill, *Phys. Rev. Lett.* **7**, 118 (1961).
- ¹⁰J. R. Schwesyg, C. R. Phillips, K. Ioakeimidi, M. C. C. Kajiyama, M. Falk, D. H. Jundt, K. Buse, and M. M. Fejer, *Opt. Lett.* **35**, 1070 (2010).
- ¹¹P. A. Arsenev and B. A. Baranov, *Phys. Status Solidi A* **9**, 673 (1972).
- ¹²A. Gröne and S. Kapphan, *J. Phys.: Condens. Matter* **7**, 6393 (1995).
- ¹³A. Förster, S. Kapphan, and M. Wöhlecke, *Phys. Status Solidi B* **143**, 755 (1987).
- ¹⁴D. Maxein and K. Buse, *J. Holography Speckle* **5**, 275 (2009).
- ¹⁵L. Kovács, K. Lengyel, and V. Szalay, *Opt. Lett.* **36**, 3714 (2011).
- ¹⁶D. A. Bryan, R. Gerson, and H. E. Tomaschke, *Appl. Phys. Lett.* **44**, 847 (1984).
- ¹⁷Y. Furukawa, K. Kitamura, A. Alexandrovski, R. K. Route, M. M. Fejer, and G. Foulon, *Appl. Phys. Lett.* **78**, 1970 (2001).
- ¹⁸L. Kovács, M. Wöhlecke, A. Jovanovic, K. Polgar, and S. Kapphan, *J. Phys. Chem. Solids* **52**, 797 (1991).
- ¹⁹Y. Shepelev, R. Bubnova, S. Filatov, N. Sennova, and N. Pilneva, *J. Solid State Chem.* **178**, 2987 (2005).
- ²⁰P. K. Gallagher, H. M. O’Bryan, E. M. Gyorgy, and J. T. Krause, *Ferroelectrics* **75**, 71 (1987).
- ²¹Y. Wang, Y. J. Jiang, Y. L. Liu, F. Y. Cai, and L. Z. Zeng, *Appl. Phys. Lett.* **67**, 2462 (1995).
- ²²V. V. Maslyuk, T. Bredow, and H. Pfnür, *Eur. Phys. J. B* **42**, 461 (2004).
- ²³V. Zhdanova, V. Klyuev, V. Lemanov, I. Smirnov, and V. Tikhonov, *Phys. Solid State* **10**, 1725 (1968).
- ²⁴H. M. Lai and K. Young, *J. Acoust. Soc. Am.* **72**, 2000 (1982).
- ²⁵J.-M. Heritier, *Opt. Commun.* **44**, 267 (1983).